

ZnO and SiO₂ Nano Particles as Intermediate Coatings for Superhydrophobic and Whiter Self-Clean Polished Porcelain Tiles

H. R. Abdi Rokn Abadi¹, M. Khajeh Aminian^{*1}, Salar K. Fatah²

¹ Nano Pigments and Coatings Laboratory, Department of Physics, Yazd University, P.O. Box: 89195-741, Yazd, Iran

² Department of Physics, College of Education, University of Garmian, Kalar-Kurdistan Region, P.O. Box: 70-236, Iraq

ARTICLE INFO

Article history:

Received: 24 May 2024

Final Revised: 12 Aug 2024

Accepted: 17 Aug 2024

Available online: 31 Aug 2024

Keywords:

Ceramic tile

Super hydrophobic

Antifouling

Contact angle

Nano-polished

Wetting

ABSTRACT

Traditional porcelain tiles often lack self-cleaning properties and suffer from aesthetic limitations. This study presents a novel approach for fabricating superhydrophobic, self-cleaning porcelain tiles with enhanced visual appeal. We strategically combined SiO₂ and ZnO nanolayers with an antifouling material, applied via spray and drop coating methods. Characterizations (FE-SEM, FTIR, contact angle, UV-Vis, colorimetry, roughness, illuminance, and stain resistance) confirmed the effectiveness of our approach. Heat treatment of the antifouling coating (400 °C) significantly increased hydrophobicity (WCA=119°). SiO₂ and ZnO intermediate layers enhanced water repellency, achieving 154° and 149° water contact angles, respectively. This demonstrates superhydrophobicity, in line with Cassie-Baxter's model, and mimics the lotus leaf's self-cleaning mechanism. Low surface energy, likely due to antifouling nanoparticle bonds, contributes to water repellency with roll-off angles of 6° and 7° and causes anti-stain properties on the tile surface. Importantly, these layers optimize surface roughness, boosting hydrophobicity and improving the whiteness and brightness of polished tiles. Surface roughness values of 308 nm (SiO₂) and 158 nm (ZnO), along with superior whiteness values (116.4 and 106, respectively), were observed, exceeding surfaces without intermediate layers (57.5). Rayleigh scattering theory explains the whiteness enhancement. Stain resistance significantly improved with intermediate layers, while surface gloss remained unchanged. This research demonstrates the potential of our coating approach to create highly functional and visually appealing polished tiles for diverse industrial applications. Prog. Color Colorants Coat. 18 (2025), 113-128© Institute for Color Science and Technology.

1. Introduction

Nature showcases a diverse array of surfaces with remarkable properties, inspiring the development of artificial counterparts. For instance, the lotus leaf, banana leaf, and Namib Desert beetle exhibit impressive hydrophobicity, repelling water and maintaining pristine surfaces [1-5]. Driven by these natural phenomena,

scientists have pursued the creation of artificial superhydrophobic surfaces with potential applications in protecting historical structures, modifying surface performance, and developing self-cleaning, anti-bacterial, and anti-slip coatings [6-10].

Among common building materials, ceramic tiles offer considerable potential for such advancements.

*Corresponding author: * kh.aminian@yazd.ac.ir

<https://doi.org/10.30509/pccc.2024.167327.1303>

While polished tiles boast an aesthetically pleasing appearance with high gloss and hardness, their susceptibility to staining poses a significant challenge, particularly in high-traffic areas [11, 12]. This vulnerability stems from the presence of open pores on the polished surface, readily absorbing liquids and harboring dirt, thus compromising both the beauty and functionality of the tiles [13-18].

Surface properties, including surface energy, hydrophobicity, and roughness, are crucial in determining how materials interact with liquids [19-22]. Recognizing this, researchers have explored incorporating various materials into ceramic tiles to achieve functionalities like self-cleaning, anti-bacterial, and anti-slip properties [23-28]. Notably, anti-stain properties are highly desirable for floors and walls in various settings, including homes, stores, and commercial buildings [29].

Achieving stain-resistant surfaces relies on precise control over surface energy, which can be manipulated by influencing hydrophobicity, physico-chemical properties, and roughness [30, 31]. Polished and self-cleaning tiles exemplify the growing demand for surfaces with anti-stain and hydrophobic characteristics [11, 12]. Polished porcelain tiles, known for their superior gloss and hardness compared to natural stones, have witnessed significant market growth [32]. However, studies on tile polishing highlight that while the process enhances aesthetics, it can also expose previously covered pores, rendering the tiles susceptible to stains and loss of shine upon contact with liquids like coffee or tea [32-34].

Several researchers have explored methods to achieve high water repellency on ceramic surfaces. Motlagh et al. used a two-layered silica coating with varying particle sizes and a final chemical compound layer, achieving good water repellency but potentially introducing complexities for industrial applications [35]. Zheng et al. employed a laser treatment for a high contact angle, but this method likely would not be cost-effective for mass production [36]. Acikbas et al. developed a technique for wall tiles that involved adding a specific powder to the glaze and then spraying a polymer, achieving good water repellency but potentially impacting the production quality of porcelain floor tiles [37]. These studies highlight the existing efforts to create water-repellent ceramics, but limitations in cost, complexity, or applicability to

specific tile types remain challenging.

To overcome limitations of traditional tiles, this research explores a novel approach utilizing nanomaterial coatings on nano-polished tile surfaces. Strategically, ZnO and SiO₂ nanoparticles are employed as intermediate layers to enhance the final product's hydrophobicity (water repellency) and whiteness. These materials were chosen for their advantageous combination of properties: inherent whiteness that complements the aesthetics of the ceramic coating, ensuring a visually cohesive final product. Furthermore, ZnO and SiO₂ are readily available and cost-effective for large-scale production. Importantly, these intermediate layers also exhibit good adhesion properties with ceramic materials, creating a strong and durable bond between the layers. Through comprehensive characterization techniques like FE-SEM, FTIR, contact angle measurement, UV-Vis spectroscopy, colorimetry, roughness analysis, illuminance measurement, and stain resistance testing, we will evaluate the effectiveness of this approach. Our surface roughness and morphology analysis will provide insights into how these nanoparticles influence the desired properties. This research holds promise for advancing the development of high-performance tiles, offering improved durability, stain resistance, and aesthetics for diverse residential and commercial applications.

2. Experimental

2.1. Materials

The experiment utilized various components. Porcelain ceramic tiles served as the foundational substrate, with their specific glaze composition documented in Table 1 from Eefa Ceram Co. Two precursor materials were employed: nano zinc oxide (ZnO) powder (30-50 nm particle size) (98.5 % purity, Shahin Rouy Sepahan Co., Iran) and nano silicon dioxide (SiO₂) powder (30-40 nm particle size) (Isatis Co., Iran). The antifouling agent was APX-128 (Foshan Boer Ceramic Technique-China, 28 wt. %), a commercially available dispersion of silica gel nanoparticles and silicon polymers in heptane (C₇H₁₆) commonly used in ceramic tile production for surface cleaning [26]. Distilled water was the solution to prepare the ZnO coating, while ethanol served the same purpose as the SiO₂ coating.

Table 1: The composition of materials used in the glaze of porcelain tile (produced in Eefa Ceram Co.)

Glaze composition	SiO ₂	Al ₂ O ₃	CaO	B ₂ O ₃	K ₂ O	Na ₂ O
Percent (%)	61	10.5	12	3.5	6.5	6.5

2.2. Method

This study thoroughly explored the impact of various combinations of coatings and heating on porcelain ceramic tile surfaces, as shown in Figure 1. Key details about sample preparation and treatments are provided in Table 2 for clarity.

2.2.1. Substrates and pre-treatment

All experiments began with porcelain ceramic tile samples measuring 2 cm by 2 cm. Initially, these samples were subjected to a pre-heating stage at a temperature of 1200 °C for 80 minutes. This step was essential to ensure a uniform base for all subsequent treatments. Following this, the surface of the samples was polished using a BMR (LEVIGA) machine, with the process parameters set to 4.8 m/min, 3 bar, and 500 rpm.

2.2.2. Sample treatments

S1: This sample received the APX-128 antifouling

material directly applied via the drop method (two drops by using a plastic pipette) without any additional heating (designated as "antifouling coating"). To find the optimal heating temperature for hydrophobicity, seven additional coated samples with APX-128 were heated at different temperatures: 100, 200, 300, 400, 500, 600, and 700 °C for 10 minutes each. The sample heated at 400 °C is named S2.

S2: As mentioned above, this sample received the same APX-128 coating as S1 but with an additional heating step at 400 °C for 10 minutes ("antifouling coating (400 °C)").

S3 and S4: These samples explored alternative coatings using nanoparticles. S3 was coated with SiO₂ nanoparticles (0.1 g per 50 mL ethanol), while S4 received ZnO nanoparticles (0.1 g per 50 mL distilled water). Both samples were applied using the spray method with 40 coats. S3 and S4 were heated at 600 °C for 10 minutes ("alternative nanoparticle coatings").

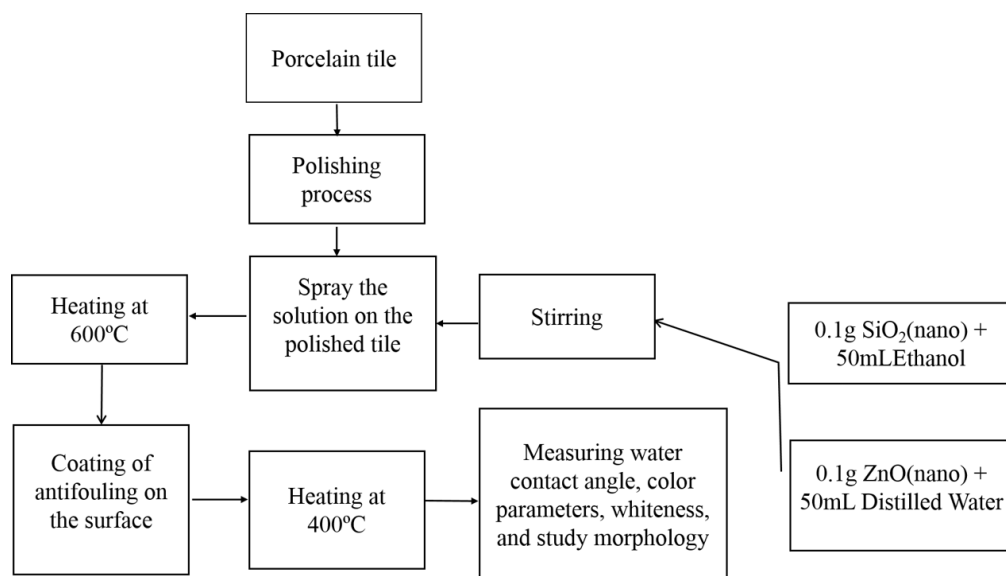


Figure 1: Schematic representation of the preparation and application process of SiO₂ and ZnO solutions for coating polished tile surfaces.

Table 2: Identifying samples: coatings and heating conditions.

No.	Sample name	Code
1	Porcelain tile	S
2	Polished tile	S0
3	Polished tile/ AF (without calcination) (drop method)	S1
4	Polished tile/ AF(400 °C) (drop method)	S2
5	Polished tile/ SiO ₂ (600 °C)	S3
6	Polished tile/ ZnO(600 °C)	S4
7	Polished tile/ SiO ₂ / AF(400 °C) (drop method)	S5
8	Polished tile/ ZnO/ AF(400 °C) (drop method)	S6

S5 and S6: To investigate combined effects, S3 (first coated with SiO₂ nanoparticles) received an additional layer of APX-128 via the drop method before heating at 400°C for 10 minutes (designated as "S5, combined coating"). Similarly, S4 (initially treated with ZnO nanoparticles) received a subsequent APX-128 layer and heating at 400 °C for 10 minutes (designated as "S6, combined coating").

2.3. Characterization techniques

FE-SEM imaging (TeScan-Mira III 30 kW) revealed the surface morphology. FT-IR spectroscopy (Bruker FT-IR Equinox 55) identified chemical bonds (500-4000 cm⁻¹). UV-Vis spectroscopy (Ocean Optic HR400) determined optical properties (200-850 nm). Colorimetry (CIE Lab) also quantified visual appearance (L*, a*, b*). The surface roughness of the coated tiles was investigated using a Perthometer M2-Mahr GmbH-Gottingen-Germany roughness tester. This measurement, expressed as the average arithmetic roughness (Ra), provided valuable information about the texture of the coatings and their potential impact on contact angle and adhesion properties. Contact angle measurements were performed using a Dino-Lite digital microscope and Digimizer software. This technique involved placing a water droplet (55 µL) on the coated surface and measuring the angle between the droplet and the surface. The illuminance of the coated surfaces was measured using an 18-1407 LUX meter at a 60° angle. This assessment provided insights into the coatings' light reflection and scattering properties, which are relevant for potential applications in light-sensitive environments. The anti-staining performance of the coatings was evaluated following the INSO 9169-14 standard. This standard

prescribes specific stains like olive oil, alcohol-iodine, and glyceryl tributyrate-chromium oxide. After application, the stains were removed with water and various detergents. This evaluation provided valuable information about the ability of the coatings to resist staining from common household and industrial contaminants.

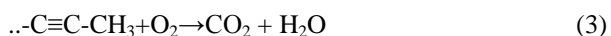
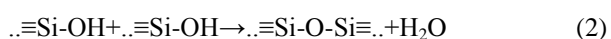
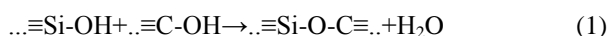
3. Results and Discussion

Figure 2 illustrates the influence of the heating process on the water contact angle (WCA) of the antifouling-coated surface (S1). As observed, the initial WCA of the surface at room temperature was approximately 89°. Interestingly, the WCA continuously increased with increasing temperature until reaching a maximum of 119° at 400 °C. However, further temperature elevation beyond 400 °C resulted in a notable decrease in the WCA. While heat treatment can enhance the coating's water repellency by potentially reorienting polymer chains, removing hydrophilic groups, or altering surface texture, excessive heat can be detrimental. It could break down polymers, increase surface energy, weaken the coating-substrate bond, and negatively impact wettability through delamination or surface changes.

FTIR was employed to analyze the surface composition and chemical modifications of an antifouling material subjected to thermal treatment. The material, previously identified as a dispersion of silica gel nanoparticles and silicon polymers in heptane (C₇H₁₆), underwent drying at room temperature followed by heating at 400 and 600 °C. Detailed results are presented in Figure 3. The FTIR spectra revealed significant changes upon heating. Notably, alkane and

alkyne functionalities, identified by peaks at 2966 and 2179 cm⁻¹, decreased in intensity. The complete disappearance of the alkyne-related peaks (2179 and 2357 cm⁻¹) at 600 °C suggested extensive thermal decomposition.

Additionally, the intensity of the C-H peak (813 cm⁻¹) decreased with increasing heating temperature, further supporting the removal of organic moieties from the surface. Conversely, the intensity of Si-O-Si and Si-O-C peaks (770-1450 cm⁻¹) increased with heating, indicating the formation of new bonds between the silica nanoparticles and the silicon polymers. This likely resulted in a more "ceramic-like" surface with more inorganic Si-O bonds. Three potential reactions involving condensation and oxidation processes have been proposed to explain the observed changes. These reactions contribute to the thermal transformation of the material, potentially leading to enhanced antifouling properties observed at higher temperatures (Eqs. 1-3).



The influence of various treatments on the surface properties of different samples is evident in their water contact angles, presented in both Table 3 and Figure 4.

Table 3 summarizes the contact angle data, while Figure 4 visually represents all samples. Also, the color pictures of drops on the samples have been shown in supplementary materials. Uncoated porcelain tiles (S) exhibit hydrophilic with a contact angle of 65°, while polished porcelain tiles (S0) are slightly more hydrophilic with an angle of 53°. Coating a polished tile with the antifouling material (S1) further increases its water repellency, evidenced by a higher contact angle of 89°.

Interestingly, heat treatment amplifies this effect, as demonstrated by the significant increase in S2's contact angle to 119° after heating at 400°C. This highlights the combined impact of the antifouling coating and heating in enhancing hydrophobicity. In contrast, nanolayer coatings of SiO₂ and ZnO (S3 and S4) induce super hydrophilic characteristics, achieving contact angles below 10°. This indicates excellent water adhesion, showcasing a contrasting behavior compared to the hydrophobic samples. Notably, applying the antifouling material via the drop method and subsequent heating at 400°C (S5 and S6) reverses this trend, resulting in remarkable water repellency. These samples boast superhydrophobic surfaces with exceptionally high contact angles (154° and 149°) and low roll-off angles (6° and 7°), signifying their superior ability to repel water.

Table 3: Water contact angles and roll-off angles of samples (WCA data is an average of 10 contact angle measurements).

No.	Sample	Coating method	WCA (Water Contact Angle)	Standard deviation (°)	Roll off angle	Surface property
1	S	None	65°	4.32	-	Hydrophilic
2	S0	None	53°	8.10	-	Hydrophilic
3	S1	AF-drop (without calcination)	89°	8.14	-	Hydrophilic
4	S2	AF-drop (after heating at 400°C)	119°	5.28	-	Hydrophobic
5	S3	SiO ₂ nanolayer (spray)	<10	-	-	Superhydrophilic
6	S4	ZnO nanolayer (spray)	<10	-	-	Superhydrophilic
7	S5	SiO ₂ + AF Drop method	154°	3.54	6°	Superhydrophobic
8	S6	ZnO+ AF Drop method	149°	4.72	7°	Superhydrophobic

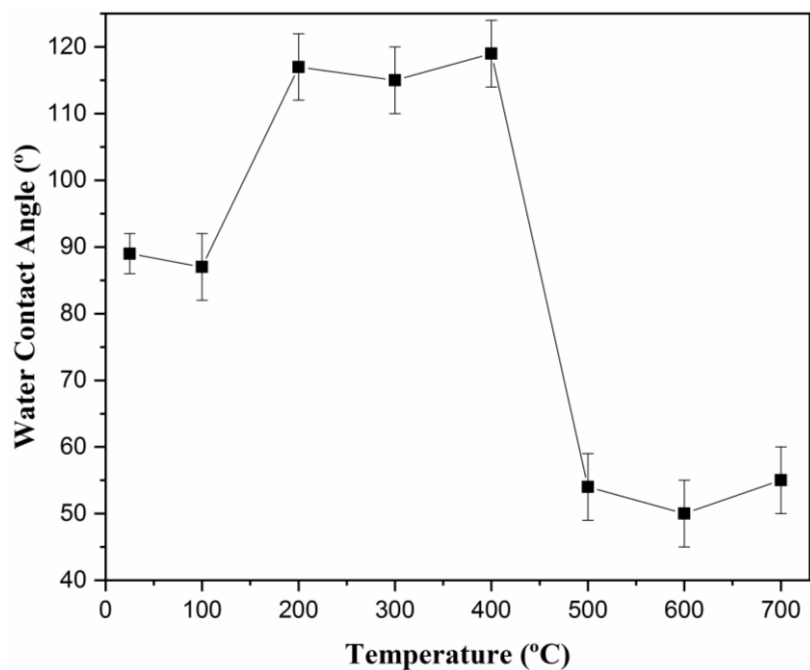


Figure 2: After thermal treatment, water contact angle measurements on the antifouling-coated samples. Each sample underwent 15 individual measurements, with the average value and an error margin of less than $\pm 5^\circ$ reported.

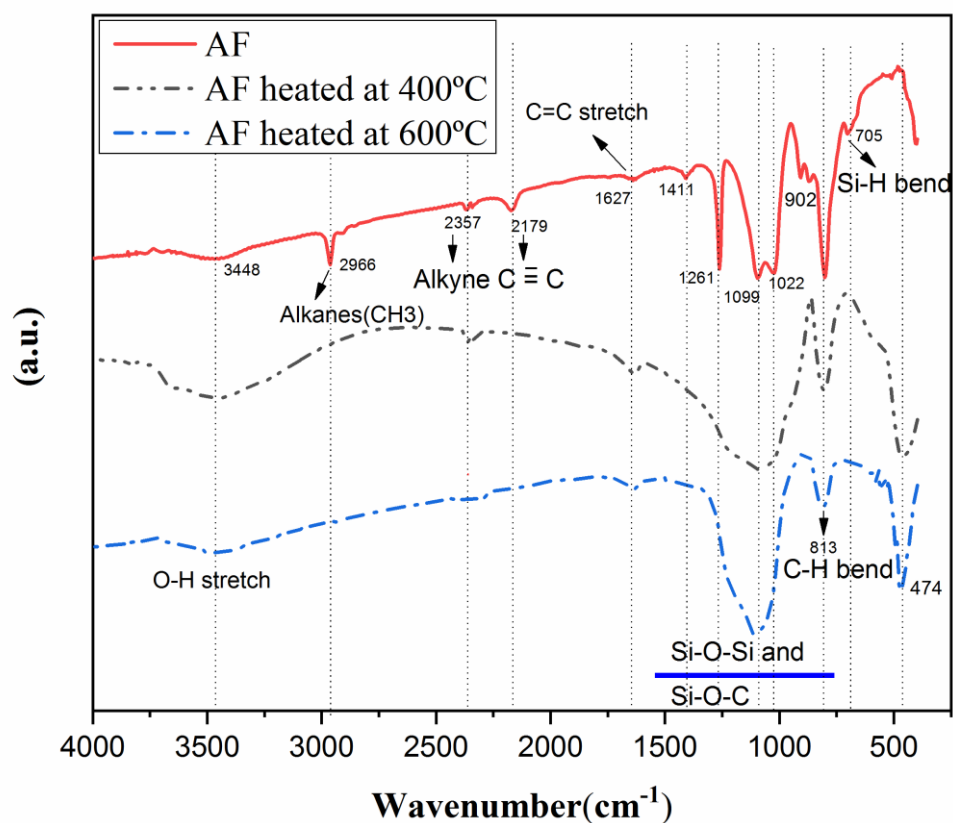


Figure 3: FTIR spectra of the antifouling material dried at room temperature and heated at 400 and 600 °C.

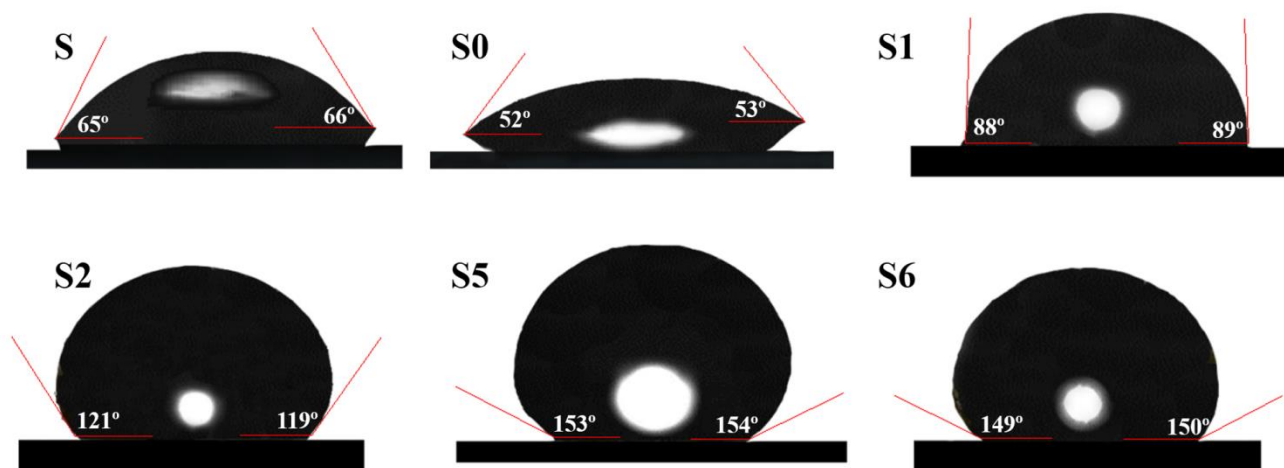


Figure 4: Contact angles of water droplets on the surface of the samples: S (Porcelain tile), S0 (Polished tile), S1 (Polished tile/AF), S2 (Polished tile/AF(400 °C)), S5 (Polished tile/ SiO₂/AF(400 °C)), and S6 (Polished tile/ZnO/AF(400 °C)). Note: Contact angles are not shown for samples S3 and S4 due to their superhydrophilic nature, where water readily spreads on the surface. A real-color image of the contact angles of the drops is available in the supplementary files.

Figure 5 presents the FE-SEM images of the different sample surfaces: S, S0, S1, and S2. Figures 5a and 4b depict the untreated porcelain surface (S) and its polished counterpart (S0). The polished surface exhibits pores that can facilitate the adsorption of pollutants, leading to surface discoloration. An antifouling coating (S1) was applied to address this issue, as shown in Figure 4c. This treatment effectively filled the pores, resulting in a decrease in surface porosity. However, heating the coated surface at 400°C (S2) induced the formation of nanoparticles and increased surface roughness (Figure 5d).

Interestingly, this roughness also generated nanometer-scale patterned structures on the surface. The combined effect of increased roughness and nanostructures led to a significant improvement in the contact angle of the surface, from 89° to 119° (Figure 5d and Table 3). The detailed impact of roughness on the contact angle will be discussed in a subsequent section. Figure 5e shows the particle size distribution of the surface of S2. The average particle size is 103 nm, indicating the formation of relatively small nanoparticles after the 400°C heat treatment.

Figures 6 and 7 unveil a two-step approach to modifying the porcelain surface for enhanced functionality, focusing on the initial nanolayer deposition (Figure 6) and subsequent antifouling treatment (Figure 7). Figures 6a and 6b showcase FE-SEM images of the deposited SiO₂ (S3) and ZnO (S4) nanolayers, respectively. Both exhibit uniform nanoparticle distributions across the surface, with sizes

ranging from 100 to 300 nm, as confirmed by the histograms in Figures 6c and 6d. The average particle size is 143 nm for SiO₂ and 170 nm for ZnO (Figure 6d). Although these layers exhibit super hydrophilicity, the absence of patterned structures, like those seen on lotus leaves, may hinder their self-cleaning abilities. Patterned structures contribute to lower surface energy, a key factor for self-cleaning surfaces.

Figure 7 addresses this limitation by introducing an antifouling treatment to S5 (SiO₂) and S6 (ZnO) followed by heat treatment at 400°C. Figure 7a reveals individual nanoparticles successfully attached to the SiO₂ surface in S5, indicating effective coating. In contrast, Figure 7b demonstrates a remarkable transformation in S6, where the ZnO surface exhibits the formation of agglomerated nanoparticle clusters remarkably resembling the patterned structures found on lotus leaves. These clusters potentially create air cushions between individual structures, reducing surface energy and promoting water droplet repellency, mimicking the self-cleaning mechanism of the natural lotus leaf [26]. The particle size distributions in Figures 7c and 7d confirm the presence of nanoparticles in both samples, with S5 exhibiting a wider range (100-700 nm, average 273 nm) compared to S6's narrower range (50-300 nm, average 175 nm). These tailored surface modifications, with their distinct nanoparticle morphologies and patterned structures (particularly evident in S6(b)), pave the way for exploring their potential applications in various fields, particularly in self-cleaning and hydrophobic surfaces.

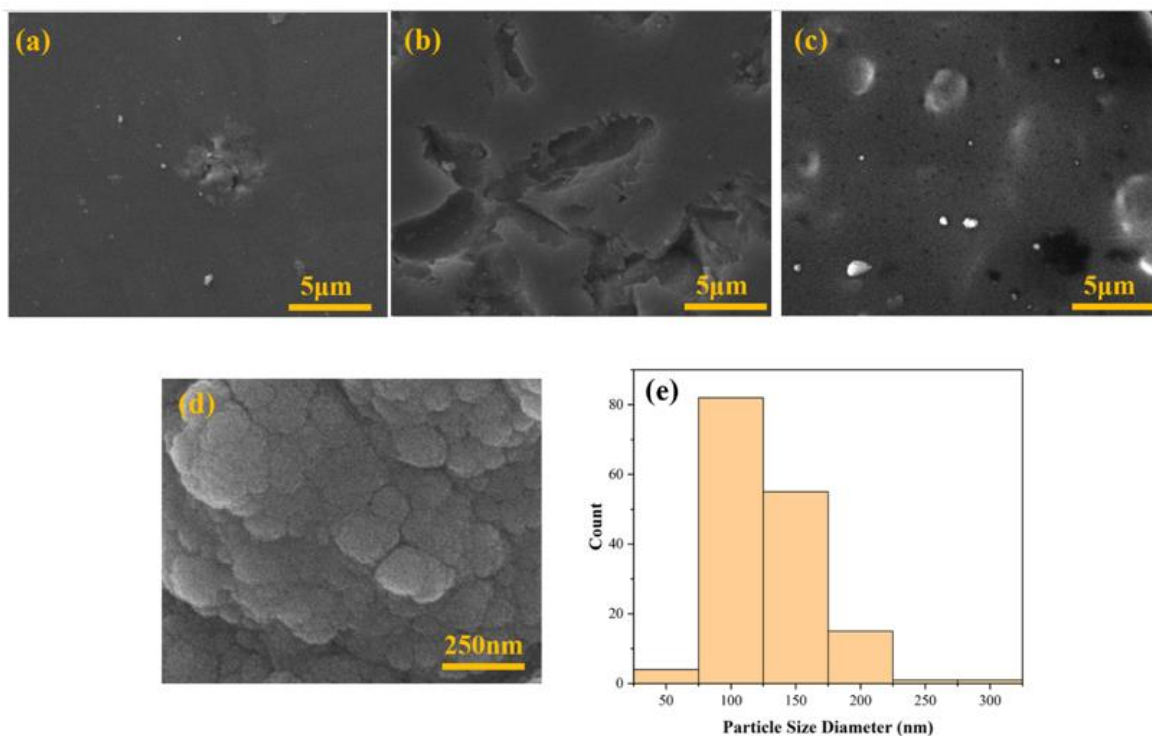


Figure 5: FE-SEM images of samples: (a) S (Porcelain tile), (b) S0 (Polished tile), (c) S1 (Polished tile/AF), (d) S2 (Polished tile/AF(400 °C)) and (e) Particle size distribution of sample S2. The average size of 156 particles is 103 nm with a standard deviation of ± 28 nm.

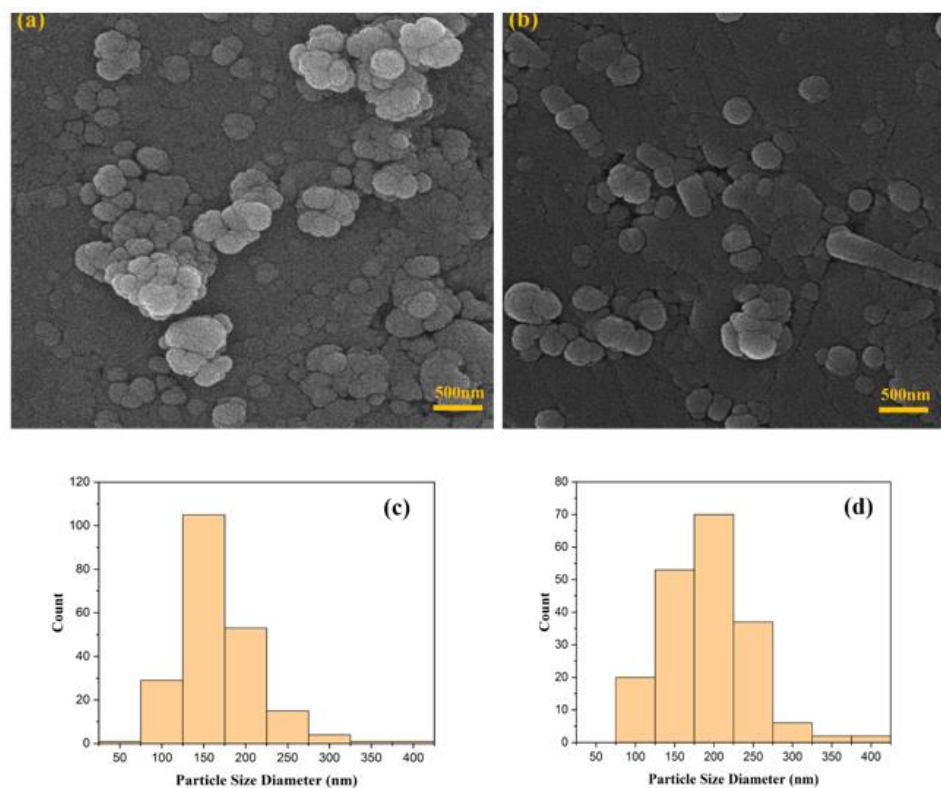


Figure 6: FE-SEM images and particle size distributions of S3 Polished tile/ SiO_2 (600 °C) (a, c) and S4 Polished tile/ZnO (600 °C) (b, d); Average sizes are 143 nm (S3, 209 particles) and 170 nm (S4, 190 particles) with standard deviations of ± 40 and ± 48 nm, respectively.

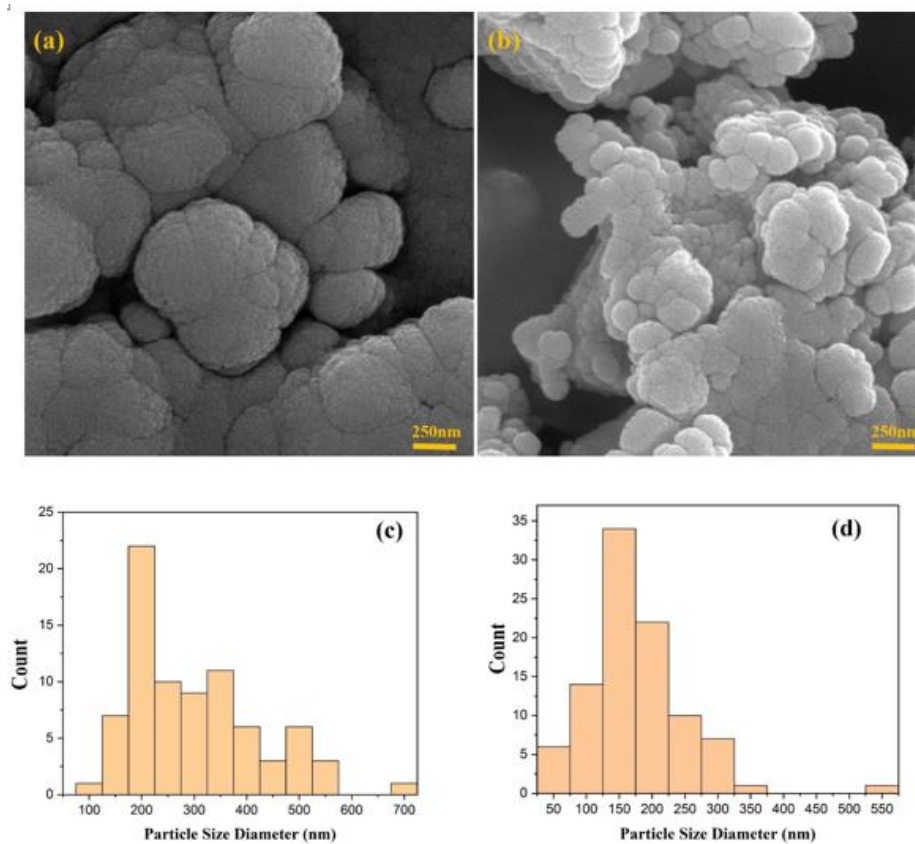


Figure 7: FE-SEM images and average particle sizes of S5 (Polished tile/ SiO₂/AF(400 °C)) (a, c) and S6 (Polished tile/ZnO/AF(400 °C)) (b, d); Average sizes are 273 nm for S5 (79 particles) and 175 nm for S6 (89 particles), with standard deviations of ±65 and ±74 nm, respectively.

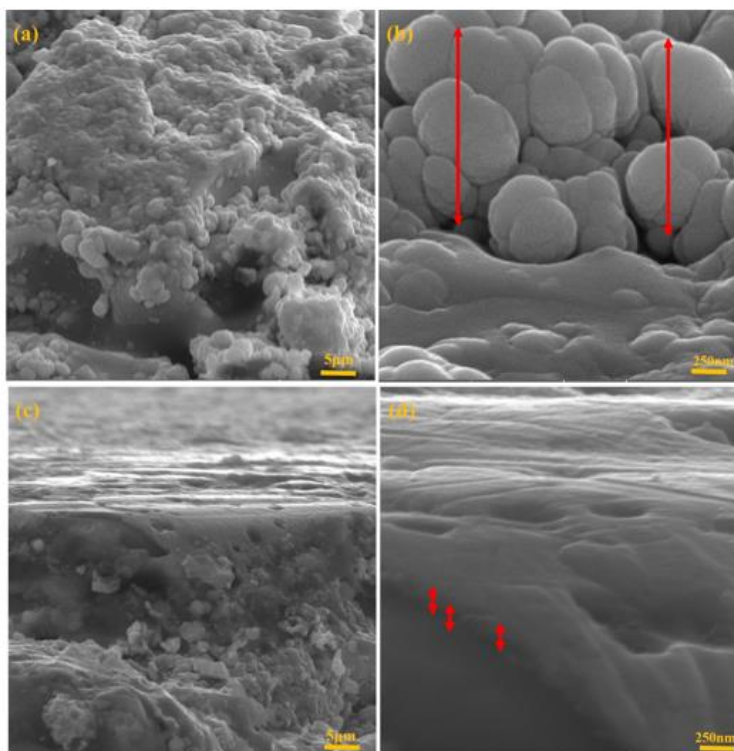
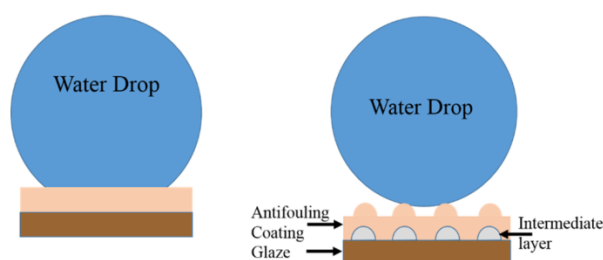


Figure 8: FE-SEM image of sample S5 (a,b) and Sample S6 (c,d) cross-sections; The average thickness of (SiO₂+antifouling) and (ZnO+antifouling) layers on the surface of samples S5 and S6 is 677 and 220 nm, respectively.

FE-SEM analysis revealed fascinating details about the coated porcelain surfaces (Figure 8). Both S5 and S6 samples exhibited multi-layered structures with well-adhered nanoparticles, comprising either SiO₂ or ZnO combined with antifouling material (Figures 8a-b and c-d), respectively. Intriguingly, the surfaces displayed a unique topography with roughness, protrusions, and depressions. This intriguing variation potentially enhances surface area and interaction with water and biomolecules, impacting functionality. Remarkably, these features were achieved with incredibly thin and uniform coatings, measuring only 677 and 220 nm for S5 and S6, respectively, making them invisible to the naked eye. This combination of multi-layered structure, adhered nanoparticles, and unique topography paves the way for further exploration of these coatings' potential applications.

Surface features significantly impact how a surface interacts with water, dictating its hydrophobicity. As shown in Scheme 1 a (S2), the water droplet fills the surface grooves, indicating strong capillary interaction and low hydrophobicity. Conversely, in Scheme 1-b, the droplet beads up. It remains suspended on air due to the significantly smaller surface features than the droplet, leading to minimal contact and high hydrophobicity, consistent with the Cassie-Baxter state [38].

The porous structure of the polished tile surface promotes water absorption and adhesion, as demonstrated by the Wenzel and Cassie transition models [39]. Surface energy plays a crucial role in achieving superhydrophobic behavior. Reducing surface energy increases the contact angle, making the surface more water-repellent [40]. Coating the surface with an antifouling agent fills the porous structure, reducing surface energy and thus increasing the contact angle. Notably, the micro/nanostructure of the surface mimics the natural superhydrophobic lotus leaf, further enhancing its water-repelling properties.



Scheme 1: (a) A scheme of S2, (b) schemes of S5 and S6. The wetting transition from the Wenzel state to the Cassie-Baxter state on the tile surface was investigated.

Surface roughness, average particle size, and water contact angle (WCA) measurements are presented in Table 4. Ra and Rz, representing the arithmetical mean deviation and average maximum height of the profile, respectively, are used to characterize surface roughness. The results indicate that applying the antifouling material (S1) to the polished tile (S0) reduced both Ra and Rz, suggesting it filled surface porosity. However, heating this layer at 400°C (S2) increased Ra and Rz, likely due to material accumulation and reaction on the surface. When heated to 400 °C, the antifouling layer (dispersion of silica gel nanoparticles and silicon polymers) undergoes thermal decomposition. This is supported by the FTIR analysis (Figure 3), which shows a decrease in the intensity of peaks associated with alkane and alkyne functionalities (2966 and 2179 cm⁻¹). This breakdown process can leave behind residual fragments or byproducts on the surface, contributing to increased roughness (Ra and Rz). Notably, Ra and Rz decreased again for samples S5 and S6 compared to S2, implying that pre-coating with SiO₂ and ZnO nanoparticles filled some surface porosity. The WCA data in Table 4 reveals that S0, S1, S3, and S4 are hydrophilic, while S2 is hydrophobic, and S5 and S6 exhibit superhydrophobicity.

Interestingly, the samples correlate with Ra, Rz, and WCA. This suggests that both surface composition and roughness influence WCA. Comparing Ra with the WCA of S2, S5, and S6 indicates that achieving superhydrophobicity may only require roughness in the nanometer range (sub-micrometer). Reflection spectra analysis (Figure 9) revealed interesting insights into our coated samples' surface light reflection properties. While uncoated (S0) and S1 samples displayed high average light reflection about 78 and 78.3 %, respectively in the visible range (400-700 nm), S2 exhibited a significant decrease (63 %), indicating a reduction in surface lightness. This highlights the impact of the heating process employed on S2 during antifouling material incorporation.

Introducing SiO₂ and ZnO nanoparticles through the coating (S5 and S6) restored the light reflection and surpassed the uncoated counterparts. S5 and S6 achieved average reflections of 77.8 and 74.3 %, respectively. This translates to a relative increase in the lightness parameter (L*) measured through colorimetry (Table 5). While S0 and S2 had L* values of 90.65 and 83.63, respectively, S5 and S6 reached 89.73 and 88.49, indicating a successful restoration of lightness

through nanoparticle coating.

Similar trends were observed for surface whiteness. Heating S1 to 400 °C in S2 drastically dropped whiteness from 83 to 57.5 (Table 5). However, coating with SiO₂ and ZnO nanoparticles (S5 and S6) led to a remarkable increase in whiteness, exceeding even the uncoated samples. S5 and S6 achieved whiteness values of 116.4 and 106, respectively, compared to 81 and 83 for S0 and S1. This significant enhancement in whiteness, coupled with the superhydrophobicity of the coated surfaces, demonstrates the high quality and potential benefits achieved through the chosen coating approach.

Based on Table 4, the average particle sizes of S2, S5, and S6 are 103, 273 and 175 nm, respectively. Rayleigh scattering theory[41] establishes that the intensity of light (electromagnetic wave) scattering is contingent upon particle size (Eq. 4):

$$I_s = \left(\frac{k^4 a^6}{r^2}\right) \left(\frac{\epsilon-1}{\epsilon+2}\right)^2 \sin^2 \theta^2 \tag{4}$$

here, k represents the wavenumber, a signifies the particle size, r denotes the distance from the origin, ε stands for the dielectric constant, and θ depicts the angle between the incident light and detection. Large particles induce greater scattering, whereas smaller particles result in reduced scattering. The predominant cause of enhanced whiteness in S5 and S6 compared to S2 appears to be the larger average particle size. As shown in Scheme 2a, in sample S2, a portion is reflected when light interacts with the surface. At the same time, another part is transmitted or absorbed through the antifouling, glaze, and engobe layers, thereby diminishing whiteness. Conversely, as illustrated in Scheme 2 b, SiO₂ and ZnO nanoparticles in samples S5 and S6 serve as scattering centers, increasing the proportion of light scattered or reflected onto the surface, with only a minor fraction transmitted through the layers for absorption. This mechanism contributes to the heightened whiteness of the surface.

Table 4: Presents the samples' roughness, average particle size, and water contact angle.

No.	Sample	Average Particle Size (nm)	Ra(nm)	Rz(μm)	WCA(°)
1	S0	-	335	5.92	53
2	S1	-	247	3.74	89
3	S2	103	801	3.81	119
4	S3	143	135	3.31	<10
5	S4	170	124	2.65	<10
6	S5	273	308	2.93	154
7	S6	175	158	1.86	149

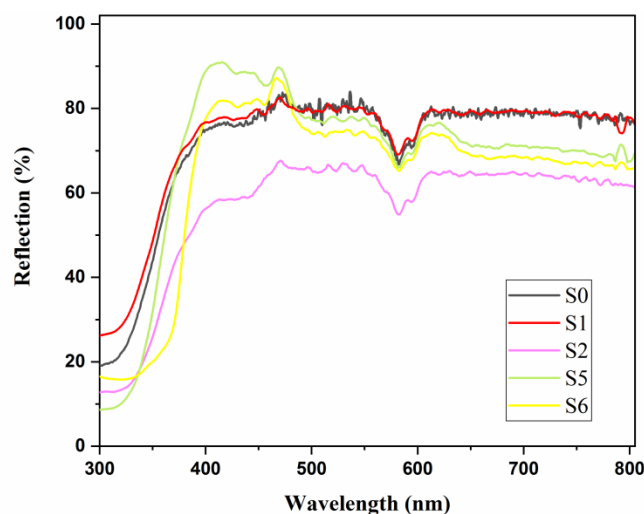
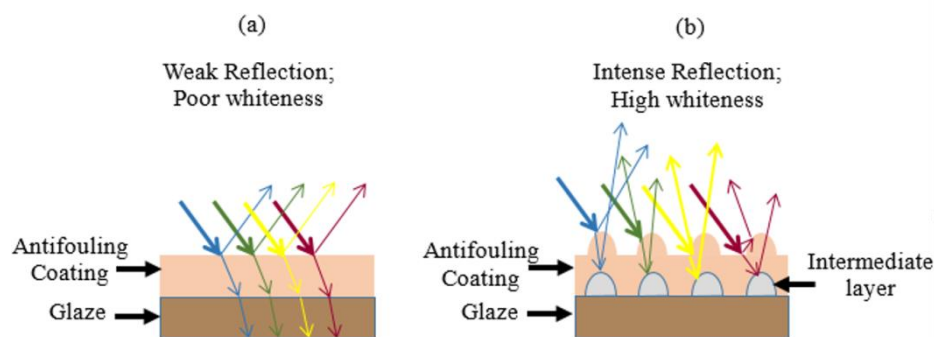


Figure 9: Reflection spectra for samples S0, S1, S2, S5, S6.



Scheme 2: Illustrates the distinct reflection behavior: (a) Weak reflection in S2 due to lack of scattering centers, leading to low whiteness and (b) Strong reflection in S5 and S6 as nanoparticles act as scattering centers, enhancing whiteness.

Table 5: The optical and colorimetric parameters alongside the water contact angle measurements.

No.	Sample	L*	a*	b*	Whiteness	WCA(°)
1	S0	90.65	-2.25	-0.69	81.0	53
2	S1	90.69	-1.59	-1.10	83.0	89
3	S2	83.63	-3.30	1.12	57.5	119
4	S3	91.02	0.39	-7.57	114.0	< 10
5	S4	91.31	1.27	-8.57	119.1	< 10
6	S5	89.73	0.40	-8.59	116.4	154
7	S6	88.49	0.04	-6.85	106.0	149

Evaluating the stability of surface hydrophobicity is crucial for achieving a perfect coating. To assess this, samples were exposed to air and water for a set period. Subsequently, the contact angle of water droplets on the surface was measured. Figure 10 presents the results of this experiment. As evident from Figure 10, there is a clear contrast in the trends observed for samples exposed to air compared to water. While samples S5 and S6 initially exhibit a high contact angle (around 155°), indicating a high degree of hydrophobicity, the contact angle for samples in water reduces significantly over time. After 24 hours of immersion, the contact angle for both S5 and S6 in water decreases to around 110°. In contrast, the contact angle for air-exposed samples remains relatively constant throughout the experiment, hovering around the initial value of 155°. This observation suggests that the coating may experience a partial loss of its water-repelling properties when exposed to water for extended periods. Possible reasons for this behavior could be the penetration of water molecules into the coating or the disruption of hydrophobic groups at the surface due to water exposure.

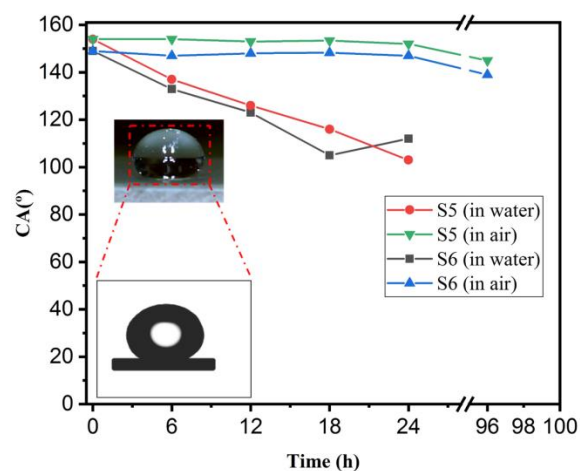


Figure 10: Stability of the hydrophobicity of the layers in water and air.

Table 6 presents the illuminance data, measured in lux, for samples S, S0, S5, and S6, utilizing an 18-1407 LUX meter positioned at a 60° angle to assess the surface gloss. This measurement angle is chosen to comprehensively evaluate the coated surfaces' light reflection and scattering characteristics. The results indicate a slight variation in the measured lux values,

with S registering at 70 lux, S0 at 78 lux, S5 at 77 lux, and S6 at 75 lux. Despite the application of coatings, the illuminance values of the samples exhibit minimal reduction, suggesting that the surface coatings do not significantly impair the reflective properties of the samples.

The stain resistance of samples S, S5, and S6 was assessed utilizing the INSO 9169-14 Iranian standard organization method, which incorporates various washing methods denoted as methods a, b, c, and d, each referenced by a corresponding number (5, 4, and so

forth) as can be seen in Figure 11. Notably, method a is regarded as the optimal washing procedure. This comprehensive evaluation involved subjecting samples to different stains commonly encountered in everyday scenarios, including olive oil, glyceryl tributyrate-chromium oxide, and alcohol-iodine, mimicking typical substances that might come into contact with surfaces. After applying stains, the samples were allowed to dry for a standardized period of 24 hours. Subsequently, cleaning was carried out using warm water (55 °C), ensuring a controlled and uniform testing environment.

Table 6: The results of the LUX meter on the surface of S, S0, S5, and S6.

Samples	S	S0	S5	S6
LUX Value (lux)	70	78	77	75

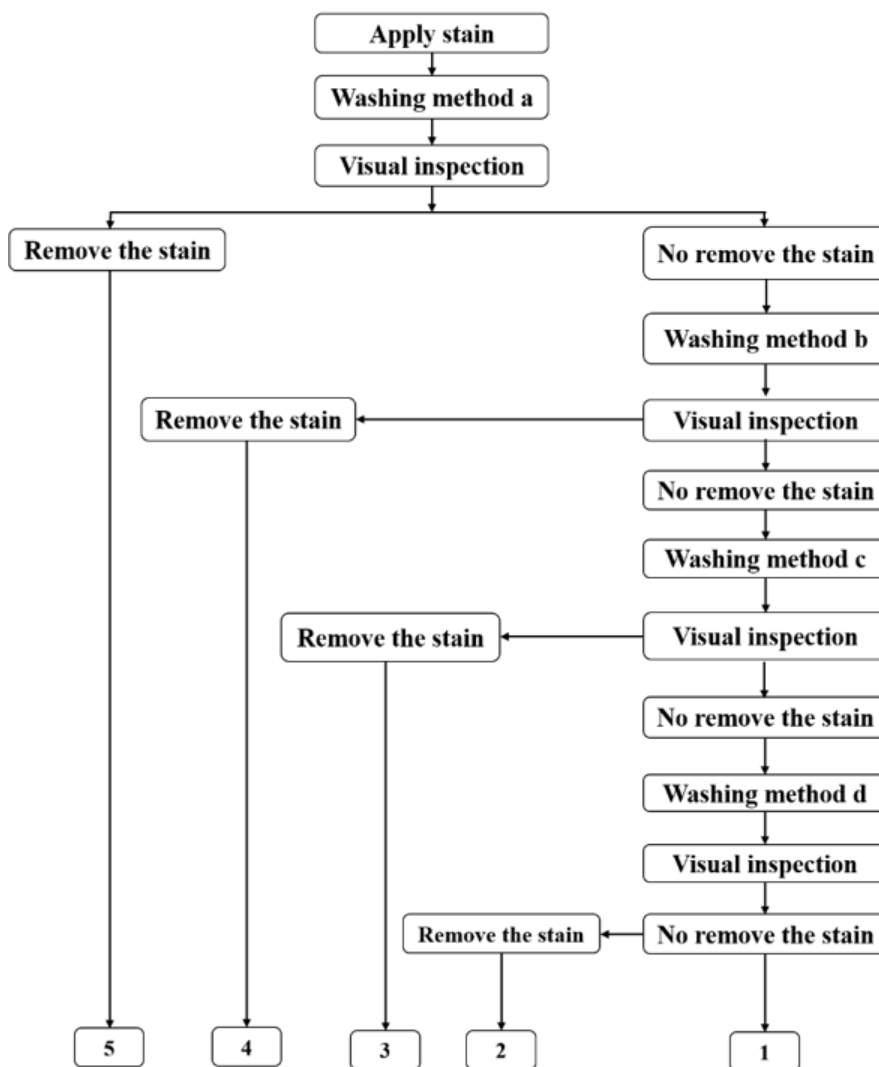
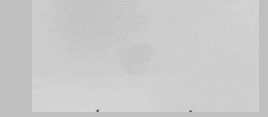
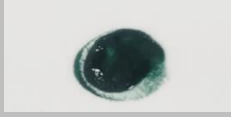
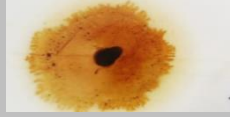
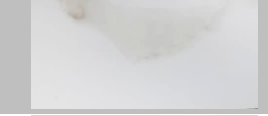
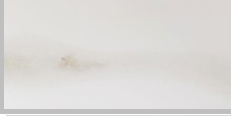

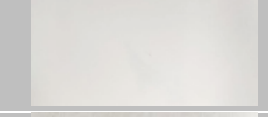
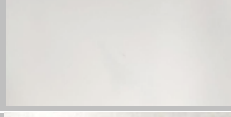
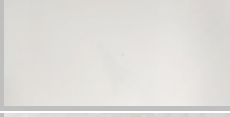


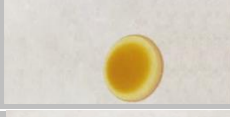
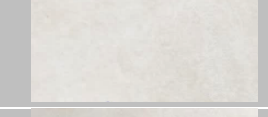
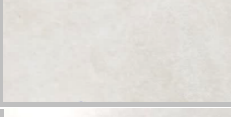
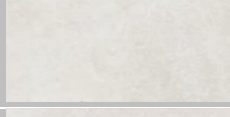
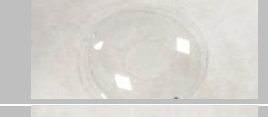
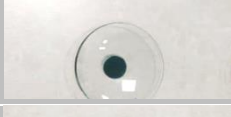
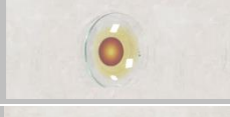
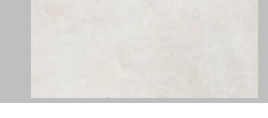
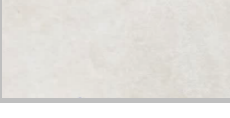
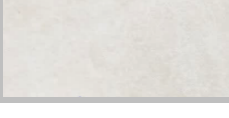


Figure 11: Illustrates the classification process for the stain resistance test according to the INSO 9169-14 Iranian standard organization.

Table 7: Presents the resistance of the samples against different stains, including olive oil, Glyceryl tributyrate-chromium oxide, and Alcohol-iodine drops.

Samples		Olive oil	Glyceryl tributyrate - Chromium oxide	Alcohol-iodine	Result
S	Before washing with method a				4 <input type="checkbox"/>
	After washing with method a				
	After washing with method b				
S5	Before washing				5 <input checked="" type="checkbox"/>
	After washing				
S6	Before washing				5 <input checked="" type="checkbox"/>
	After washing				

The testing results revealed significant differences in stain resistance among the samples, as seen in Table 7. Samples S5 and S6 demonstrated exceptional performance, achieving a stain resistance classification of class 5 when subjected to the cleaning method. This classification signifies the complete removal of stains solely through warm water washing, indicative of robust stain resistance properties. In contrast, sample S exhibited less impressive stain resistance characteristics. Upon employing method a, stains persisted on the surface of sample S, suggesting a lower level of resistance to staining compared to S5 and S6. However, method b proved effective in eliminating all stains from sample S, although requiring a more aggressive cleaning approach.

4. Conclusions

This research successfully investigated the impact of applying antifouling coatings with and without

intermediate nanolayers on polished tiles' optical, colorimetric, surface, and wetting properties. We demonstrated that our approach effectively enhances tiles' hydrophobicity and self-cleaning properties. Applying an antifouling coating on a polished tile, followed by heat treatment, significantly increased hydrophobicity. Introducing SiO₂ and ZnO intermediate layers enhanced surface roughness, leading to superhydrophobic properties with water contact angles reaching 154° and 149°, respectively. This increase in hydrophobicity is likely due to the surface morphology created by the nanoparticles enhancing the air-trapping behavior consistent with the Cassie-Baxter model. Importantly, the intermediate nanolayers remarkably improved the tiles' whiteness and L* values, surpassing tiles coated solely with antifouling material. This improvement can be explained by Rayleigh scattering due to the nanoparticle size.

Moreover, stain resistance was notably enhanced, and surface gloss remained largely unchanged, demonstrating the practical benefits of this approach. This approach offers self-cleaning and functional tiles with maintained aesthetics. Optimizing nanoparticles and durability holds the key to wider industry adoption.

5. References

- Zhu Q, Zhang C, Zhu N, Gong J, Zhou Z, Sheng D, et al. Preparation of polyester yarns with bright color and enhanced hydrophobicity using lotus leaf powders. *Ind Crops Prod.* 2023; 193:116152. <https://doi.org/10.1016/j.indcrop.2022.116152>.
- Sotoudeh F, Mousavi SM, Karimi N, Lee BJ, Abolfazli-Esfahani J, Manshadi MKD. Natural and synthetic superhydrophobic surfaces: A review of the fundamentals, structures, and applications. *Alexandria Eng J.* 2023; 68:587-609. <https://doi.org/10.1016/j.aej.2023.01.058>.
- Ge-Zhang S, Cai T, Yang H, Ding Y, Song M. Biology and nature: Bionic superhydrophobic surface and principle. *Front Bioeng Biotechnol.* 2022; 10:1-19. <https://doi.org/10.3389/fbioe.2022.1033514>.
- Xu P, Sui X, Wang S, Liu G, Ge A, Coyle TW, et al. Superhydrophobic ceramic coatings with lotus leaf-like hierarchical surface structures deposited via suspension plasma spray process. *Surf Interface.* 2023; 38:102780. <https://doi.org/10.1016/j.surfint.2023.102780>.
- Sui X, Wang Y, Sun Y, Liang W, Xue Y, Bonsu AO. Superhydrophobic behavior of cylinder dual-scale hierarchical nanostructured surfaces. *Colloids Surfaces A Physicochem Eng Asp.* 2021; 629:127406. <https://doi.org/10.1016/j.colsurfa.2021.127406>.
- Chindaprasirt P, Jitsangiam P, Pachana PK, Rattanasak U. Self-cleaning superhydrophobic fly ash geopolymer. *Sci Rep.* 2023; 13:1-9. <https://doi.org/10.1038/s41598-022-27061-6>.
- Ashok Kumar SS, Bashir S, Ramesh K, Ramesh S. A comprehensive review: Super hydrophobic graphene nanocomposite coatings for underwater and wet applications to enhance corrosion resistance. *Flat Chem.* 2022; 31:100326. <https://doi.org/10.1016/j.flatc.2021.100326>.
- Akbari R, Mohammadzadeh MR, Khajeh Aminian M, Abbasnejad M. Hydrophobic Cu₂O surfaces prepared by chemical bath deposition method. *Appl Phys A Mater Sci Proc.* 2019; 125:1-7. <https://doi.org/10.1007/s00339-019-2470-7>.
- Zhao Y, Lei L, Wang Q, Li X. Study of superhydrophobic concrete with integral superhydrophobicity and anti-corrosion property. *Case Stud Constr Mater.* 2023; 18:e01899. <https://doi.org/10.1016/j.cscm.2023.e01899>.
- Striani R, Cappai M, Casnedi L, Esposito Corcione C, Pia G. Coating's influence on wind erosion of porous stones used in the Cultural Heritage of Southern Italy: Surface characterisation and resistance. *Case Stud Constr Mater.* 2022; 17:e01501. <https://doi.org/10.1016/j.cscm.2022.e01501>.
- Li C, Zhang G, Lin L, Wu T, Brunner S, Galmarini S, et al. Silica aerogels: from materials research to industrial applications. *Int Mater Rev.* 2023; 68:862-900. <https://doi.org/10.1080/09506608.2023.2167547>.
- Akarsu M, Burunkaya E, Tunali A, Tamsü Selli N, Arpaç E. Enhancement of hybrid sol-gel coating and industrial application on polished porcelain stoneware tiles and investigation of the performance. *Ceram Int.* 2014; 40:6533-40. <https://doi.org/10.1016/j.ceramint.2013.11.106>.
- Alves HJ, Minussi FB, Melchades FG, Boschi AO. Porosidade Susceptível ao Manchamento em Porcelanato Polido. *Cerâmica Ind.* 2009; 14:21-6.
- Ambrosi M, Santoni S, Giorgi R, Fratini E, Toccafondi N, Baglioni P. High-performance and anti-stain coating for porcelain stoneware tiles based on nanostructured zirconium compounds. *J Colloid Interface Sci.* 2014; 432:117-27. <https://doi.org/10.1016/j.jcis.2014.07.002>.
- Dondi M, Raimondo M, Zanelli C. Stain resistance of ceramic tiles. *Technology* 2008:2016-9.
- Cavalcante PMT, Dondi M, Ercolani G, Guarini G, Melandri C, Raimondo M, et al. The influence of microstructure on the performance of white porcelain stoneware. *Ceram Int.* 2004; 30:953-63. <https://doi.org/10.1016/j.ceramint.2003.11.002>.
- Abou Elmaaty TM, Sayed-Ahmed K, El Gohari MM, Noaman R. Enhancing the properties of bone China ceramics by treatment with microporous SiO₂ nanoparticles. *Chem Pap.* 2022; 76:5879-91. <https://doi.org/10.1007/s11696-022-02296-9>.
- Suvaci E, Tamsu N. The role of viscosity on microstructure development and stain resistance in porcelain stoneware tiles. *J Eur Ceram Soc.* 2010; 30:3071-7. <https://doi.org/10.1016/j.jeurceramsoc.2010.06.010>.
- Song JW, Fan LW. Understanding the effects of surface roughness on the temperature and pressure relevancy of water contact angles. *Colloid Surf A Physicochem Eng Asp.* 2023; 656:130391. <https://doi.org/10.1016/j.colsurfa.2022.130391>.
- Zhang J, Xu B, Zhang P, Cai M, Li B. Effects of surface roughness on wettability and surface energy of

Acknowledgments

The authors express their gratitude to Yazd University for the generous support, which included providing access to laboratories and essential materials.

- coal. *Front Earth Sci.* 2023; 10:1-10. <https://doi.org/10.3389/feart.2022.1054896>.
21. Aminian MK, Sajadi F, Mohammadzadeh MR, Fatah S. Hydrophilic and photocatalytic properties of TiO₂/SiO₂ nano-layers in dry weather. *Prog Color Color Coat.* 2021; 14:221–32. <https://doi.org/10.30509/pccc.2021.81721>
 22. Li K, Yao W, Liu Y, Wang Q, Jiang G, Wu Y, et al. Wetting and anti-fouling properties of groove-like microstructured surfaces for architectural ceramics. *Ceram Int.* 2022; 48:6497–505. <https://doi.org/10.1016/j.ceramint.2021.11.194>.
 23. Golshan V, Mirjalili F, Fakharpour M. Self-cleaning surfaces with superhydrophobicity of Ag-TiO₂ nanofilms on the floor ceramic tiles. *Glas Phys Chem.* 2022; 48:35-42. <https://doi.org/10.1134/S1087659622010059>.
 24. Moghaddasi Z, Mohammadzadeh MR. Synthesis and effectiveness of Cu-infused TiO₂-SiO₂ based self-cleaning and antibacterial thin-films coating on ceramic tiles. *J Sol-Gel Sci Technol.* 2022; 103:396-404. <https://doi.org/10.1007/s10971-022-05853-6>.
 25. Mili M, Hada V, Mallick T, Singhwane A, Tilwari A, Hashmi SAR, et al. Advances in nanoarchitectonics of antimicrobial tiles and a quest for anti-SARS-CoV-2 tiles. *J Inorg Organomet Polym Mater.* 2022; 32:3355-67. <https://doi.org/10.1007/s10904-022-02325-w>.
 26. Fatah SK, Khajeh Aminian M, Bahamirian M. Multifunctional superhydrophobic and cool coating surfaces of the blue ceramic nanopigments based on the heulandite zeolite. *Ceram Int.* 2022; 48:21954-66. <https://doi.org/10.1016/j.ceramint.2022.04.178>.
 27. Ferreira-Neto EP, Ullah S, Martinez VP, Yabarrena JM, Simões MB, Perissinotto AP, et al. Thermally stable SiO₂@TiO₂ core@shell nanoparticles for application in photocatalytic self-cleaning ceramic tiles. *Mater Adv.* 2021; 2:2085-96. <https://doi.org/10.1039/d0ma00785d>.
 28. Reinosa JJ, Romero JJ, Jaquotot P, Bengochea MA, Fernández JF. Copper based hydrophobic ceramic nanocoating. *J Eur Ceram Soc.* 2012; 32:277-82. <https://doi.org/10.1016/j.jeurceramsoc.2011.08.013>.
 29. Motlagh NV, Derogar S, Bagherzade G, Gholami R. Preparation and characterization of anti-stain self-cleaning coating on ceramic. *Mater Chem Phys.* 2022; 276:125278. <https://doi.org/10.1016/j.matchemphys.2021.125278>.
 30. Jisr RM. Controlling Surface Energy in Polyelectrolyte Multilayers. Florida State University, 2007.
 31. Farrokhbin M, Aminian MK, Motahari H. Wettability of liquid mixtures on porous silica and black soot layers. *Prog Color Color Coat.* 2020; 13:239-49. <https://doi.org/10.30509/pccc.2020.81645>
 32. Sánchez E, García-Ten J, Sanz V, Moreno A. Porcelain tile: Almost 30 years of steady scientific-technological evolution. *Ceram Int.* 2010; 36:831-45. <https://doi.org/10.1016/j.ceramint.2009.11.016>.
 33. Hutchings IM, Xu Y, Sánchez E, Ibáñez MJ, Quereda MF. Development of surface finish during the polishing of porcelain ceramic tiles. *J Mater Sci.* 2005; 40:37-42. <https://doi.org/10.1007/s10853-005-5684-3>.
 34. Xiong H, Shui A, Shan Q, Zeng S, Xi X, Du B. Foaming mechanism of polishing porcelain stoneware tile residues via adding C, Al and Si powder. *J Eur Ceram Soc.* 2022; 42:1712-21. <https://doi.org/10.1016/j.jeurceramsoc.2021.11.065>.
 35. Motlagh NV, Derogar S, Bagherzade G, Gholami R. Preparation and characterization of anti-stain self-cleaning coating on ceramic. *Mater Chem Phys.* 2022; 276:1-11. <https://doi.org/10.1016/j.matchemphys.2021.125278>.
 36. Zheng J, Qu G, Yang B, Wang H, Zhou L, Zhou Z. Facile preparation of robust superhydrophobic ceramic surfaces with mechanical stability, durability, and self-cleaning function. *Appl Surf Sci.* 2022; 576:151875. <https://doi.org/10.1016/j.apsusc.2021.151875>.
 37. Acikbas G, Calis Acikbas N, Ubay E, Karaer H. The influence of varying Cu doping concentrations on the microstructure, phase evolution and surface wettability of ceramic glazes modified with nano Cu-ZnO. *Appl Phys A Mater Sci Proc.* 2024; 130:1-13. <https://doi.org/10.1007/s00339-024-07546-z>.
 38. Mazumder A, Alangi N, Sethi S, Prabhu KN, Mukherjee J. Study on wettability of plasma spray coated oxide ceramic for hydrophobicity. *Surf Interface.* 2020; 20:100591. <https://doi.org/10.1016/j.surfin.2020.100591>.
 39. Valipour M. N, Birjandi FC, Sargolzaei J. Super-non-wettable surfaces: A review. *Colloids Surfaces A Physicochem Eng Asp.* 2014; 448:93-106. <https://doi.org/10.1016/j.colsurfa.2014.02.016>.
 40. Sanabria-Mafaile J, San Martin-Martinez E, Cruz-Orea A. Thermal properties of superhydrophobic films applied in ceramic tiles. *Colloid Surf A Physicochem Eng Asp.* 2020; 607:125524. <https://doi.org/10.1016/j.colsurfa.2020.125524>.
 41. Guenther BD, Steel DG. Encyclopedia of modern optics. vol. 1-5. 2018. <https://doi.org/10.5860/choice.43-0036>.

How to cite this article:

Abdi Rokn Abadi HR, Khajeh Aminian M, Fatah SK. ZnO and SiO₂ Nano Particles as Intermediate Coatings for Superhydrophobic and Whiter Self-Clean Polished Porcelain Tiles. *Prog Color Colorants Coat.* 2025;18(1):113-128. <https://doi.org/10.30509/pccc.2024.167327.1303>.

